A COMPARISON OF SCATTERING RESULTS

OBTAINED WITH THE PERIODIC SURFACE

MOMENT METHOD AND SEVERAL

APPROXIMATE SCATTERING THEORIES

USING WAVE-TANK DATA

By

BRENT O'LEARY

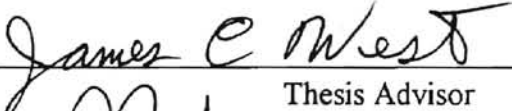Bachelor of Science

Oklahoma State University

Stillwater, Oklahoma

1993

Submitted to the Faculty of the
Graduate College of
Oklahoma State University
In Partial Fulfillment of
the Requirements for
the Degree of
MASTER OF SCIENCE
July, 1996

A COMPARISON OF SCATTERING RESULTS

OBTAINED WITH THE PERIODIC SURFACE

MOMENT METHOD AND SEVERAL

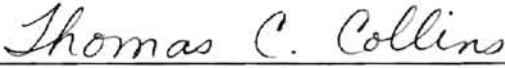APPROXIMATE SCATTERING THEORIES

USING WAVE-TANK DATA

Thesis Approved:

James C. West
Thesis Advisor

R. Ramakumar.

George Scheets

Thomas C. Collins
Dean of the Graduate College

ACKNOWLEDGMENTS

I would like to extend thanks to the people who have helped me throughout graduate school. To my advisor Dr. James West for his long-distance help and his willingness to answer my e-mail at any time regardless of how misguided the inquiry. I would like to profusely thank my office-mate Mike Sturm for the invaluable conversations and especially for allowing me the use of his master's thesis as a template for mine. I would also like to thank my committee members, Dr. Ramakumar, and Dr. Scheets for taking time to review this work.

This thesis is dedicated to my wife Tina, and son, Chandler. To my wife for her understanding as I labored on this after coming home from work, and to my son for giving me inspiration to complete this paper.

TABLE OF CONTENTS

LIST OF TABLES

LIST OF FIGURES

NOMENCLATURE

SPM	Small Perturbation Method
KA	Kirchoff Approximation
PSMM	Periodic Surface Moment Method
EFIE	Electric Field Integral Equation
MFIE	Magnetic Field Integral Equation
HH	Horizontal Polarization
VV	Vertical Polarization

CHAPTER 1

INTRODUCTION

The most limiting factor in the performance of over-sea radar systems is usually the surface-scatter clutter. This clutter can give high energy return signals which can overwhelm the signal returned from actual targets, such as ships and low flying aircraft, or cause false alarms when no target is present. The random roughness of the sea surface is responsible for this clutter. Full understanding of the surface scattering mechanism that leads to clutter signals will aid in the development of detection algorithms that can extract true signals from the clutter, reducing both the number of missed targets and the false alarm rates of such radars.

There are several analytically derived models to predict the radar backscatter from rough surfaces, each of which are valid under certain conditions. The most popular of these theories are the small perturbation method (SPM) [Rice 1958], Kirchoff (or physical optics) approximation (KA) [Beckman and Spizzichino 1963], and the two scale model [Wright 1968]. Because of the approximations made in the derivations of the models, each is rigorously valid only under certain conditions. For example, the Kirchoff approximation assumes electromagnetically large-scale roughness, gently varying surfaces (long surface correlation surface) and small to moderate incidence angles. It predicts the scattering due to the physical optics current induced on the surface of the scatterer. SPM

1

on the other hand, was derived assuming short correlation lengths and moderate incidence angles. First order SPM predicts the Bragg-resonant scattering, which is due to surface components resonant with the illuminating field's wavelength. The two scale model incorporates both of these models by applying KA to the electromagnetically large scale surface roughness and SPM to the small scale roughness. None of these models directly include the effects of surface self-shadowing, and as such, are expected to fail at the largest incidence angles (smallest grazing angles).

Despite the approximations made in their derivations, the theoretical models have often been shown to accurately predict rough-surface scattering outside of their known regions of validity. For, example, Guinard and Daley (1970) showed experimentally that the two scale model gives accurate sea-surface scattering at angles of incidence to 85° at vertical polarization. On the other hand, Chen and West (1995) showed that both SPM and KA can give accurate scattering from numerically generated surfaces at horizontal polarization and extremely large incidence angles under some surface roughness conditions. For the models to be used to their fullest potential, the true ranges of validity must be determined.

The moment method is a popular numerical technique that is often used to check the accuracy of approximate models in scattering problems [Broschat, 1993; Chen and Fung 1988; Kim et. al. 1992; Chen and West 1995]. In this approach, the moment method is used to solve electromagnetic integral equations, yielding the surface current. The surface current is then numerically re-radiated, giving the scattered field. This technique has been used to confirm the validity of the scattering theories under the conditions for

2

which they were rigorously derived [Durden and Vesecky 1990; Chen and Fung 1988; Thorsos 1988].

Unfortunately, the standard moment method is not well suited to application at the largest incidence angles. The surfaces modeled must be truncated, due to the limitations of computer speed and physical storage, leading to non-physical diffraction from the edges in the numerical scattering that can mask the real scattering, especially at small grazing angles. One way to circumvent this limitation is to apply a tapered weighting window to the incident electromagnetic field[Thorsos 1988]. This tapered window forces the excitation to zero at the edges and reduces the diffraction. This method has the limitation of not using the exact illuminating field. Also, electromagnetically valid weighting functions require longer numerically modeled surfaces with increasing incidence angles[Thorsos 1988]. At the largest incidence angles, the modeled surface must be so long that application of the moment method is cost prohibitive. A second approach is to force the surface to be periodic and include an infinite number of periods of the surface, thereby eliminating the edges in the modeled surface [Rodriguez 1990] and allowing the application of the technique at small grazing angles. The primary disadvantage of this approach is that an infinite series must be evaluated for each element of the moment interaction matrix, leading to computational inefficiency. A more efficient implementation of the periodic surface moment method was developed by Chen and West (1995), and used to investigate the validity of the scattering models from a limited class of surfaces down to grazing incidence [West et. al., 1995].

The most severe limitation in numerical studies of surface scattering is the method used to represent the scattering surface. Typically, sample surfaces are generated from an approximate power spectral density. Several roughness spectrum approximations have been used to model the ocean surface, including the power law or Phillips spectra [Phillips, 1958] and the Pierson-Moskewitz spectra [Broschat, 1993]. The Pierson-Moskewitz spectra is an approximation of the entire wave spectrum for the ocean surface, parameterized by the speed of the wind generating the waves. The power law spectra represents the saturated (large wave number) range of the Pierson-Moskewitz spectrum, and is not (to first order) a function of the wind speed. The saturated region includes Bragg-resonant energy at most frequencies. These are approximate spectra only, and as such their validity is not well established.

Only a few direct measurements of the wavenumber spectra of short ocean waves exist. These measurements are usually taken with a scanning laser slope gauge and can only resolve wave numbers from approximately 31 to 990 rad/m, which is not sufficient to resolve small capillary waves. Laboratory data from wave tanks is the only reliable source of such short wave data. There is some question of how well the results obtained with this laboratory data can be extrapolated to the field conditions found in the open sea [Jahne and Klinke, 1994].

The goal of this work is to examine the ranges of validity of the theoretical models in describing the scattering from actual water surfaces. Experimentally measured slope images taken in a closed wave tank, with wind generating waves, are integrated to obtain height profiles.

These surfaces should have roughness similar to that of open water surfaces. The scattering from upwind/downwind cuts of the surfaces is calculated using the periodic-surface moment method of Chen and West (1995). This scattering is then used to evaluate the ranges of validity of the scattering models when applied to actual water surfaces. A detailed review of the periodic surface moment method used is given in chapter two, as is a brief description of the SPM and KA scattering models. The processing of the raw surface data to allow application of the PSMM is given in chapter three, and the validity of the scattering models is examined in chapter four. Finally chapter five provides conclusions to be drawn from this effort.

CHAPTER 2
ELECTROMAGNETIC ANALYSIS

Introduction

This chapter gives an overview of the periodic-surface moment method used to predict scattering from perfectly conducting rough surfaces. The moment method is a general numerical technique used to solve linear integro-differential equations[Harrington, 1968]. When applied to rough surface scattering problems, the moment method is first applied to integral equations that force the surface boundary condition to be met, yielding the unknown surface currents. These currents can be re-radiated to give the backscattered field. Also included in this chapter is an overview of two approximate scattering theories, the Kirchoff approximation (KA) and the small perturbation model (SPM). The Kirchoff approximation re-radiates the physical optics current to get the backscattered field. The small perturbation model uses the roughness spectrum of the surface to predict the scattering due to small resonant components of the surface.

The General Scattering Problem

Figure 2.1 shows the general rough surface scattering geometry to be considered here.
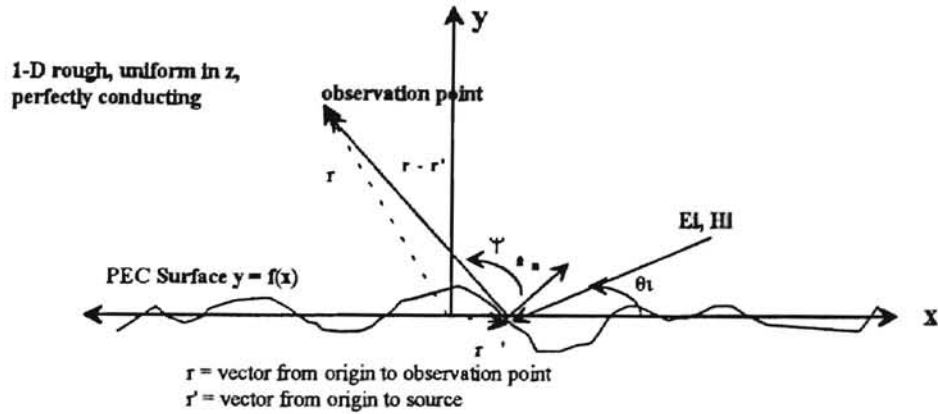
Figure 2.1 Geometry for the General Scattering Problem

Moment Method Scattering Calculations

The Electric Field Integral Equation

The scattering from a one-dimensionally rough surface is best described by the electric field integral equation when the illumination is horizontally polarized. The EFIE insures that the boundary condition

$$\mathbf{E}_{\text{tan}}^{t} = \hat{a}_{n} \times (\mathbf{E}^{s} + \mathbf{E}^{i}) = 0, \tag{2-1}$$

is met. Where $\mathbf{E}_{\text{tan}}^{t}$ is the total tangential field at the surface $\hat{a}_{n}$ is a unit vector normal to the surface, $\mathbf{E}^{s}$ is the scattered electric field, and $\mathbf{E}^{i}$ is the incident electric field. For a general, two-dimensionally rough surface the EFIE is given by [Balanis 1989]

$$j \frac{\eta}{k} \hat{a}_{n} \times [k^{2} \iint J_{s}(\mathbf{r}')G(\mathbf{r},\mathbf{r}')ds' - \iint \nabla' \cdot J(\mathbf{r}')\nabla' G(\mathbf{r},\mathbf{r}')ds'] = \hat{a}_{n} \times \mathbf{E}_{\text{tan}}^{i} \tag{2-2}$$

on S, where $\mu_{o} = 4\pi \times 10^{-7}$, $\varepsilon_{o} = \frac{1}{36\pi} \times 10^{-9}$ is , $\eta = \sqrt{\frac{\mu_{o}}{\varepsilon_{o}}}$, is the intrinsic impedance of free space, $k = \varpi \sqrt{\mu \varepsilon} = \frac{2\pi}{\lambda}$ is the electromagnetic wave number, λ is the wavelength of the incident field, ω is the radial frequency of the incident field, $\mathbf{r}$ is a vector from the origin to an observation point on the surface, $\mathbf{r}'$ is a vector from the origin to a point on the source,

7

S is the scattering surface and $G(\mathbf{r},\mathbf{r}')$ is the three dimensional form of Green's function given by

$$G(\mathbf{r},\mathbf{r}') = \frac{e^{-jkR}}{4\pi R}, \tag{2-3}$$

where R is the distance from the source point to the observation point. R is expressed in Cartesian coordinates as

$$R = |\mathbf{r} - \mathbf{r}'| = \sqrt{(x-x')^2 + (y-y')^2 + (z-z')^2} \tag{2-4}$$

The surface current density on the surface of the scatterer is found by solving equation (2-2) for $J_s(\mathbf{r}')$ using the moment method. The scattered field is then found by re-radiating the surface current using

$$\mathbf{E}^s(\mathbf{r}) = -j\mu\omega \int_s \mathbf{J}_s(\mathbf{r}')G(\mathbf{r},\mathbf{r}')ds' + \frac{1}{\varepsilon\omega}\nabla\int_s \nabla'\cdot\mathbf{J}_s(\mathbf{r}')G(\mathbf{r},\mathbf{r}')ds' \tag{2-5}$$

This re-radiation equation can be simplified for a one dimensionally rough scattering surface with a horizontally polarized incident field. In this case the scattering surface is described as $y = f(x)$. The incident electric field $\mathbf{E}^i$ has only a z component, and the scattered electric fields are uniform in z.

Thus using,

$$\int_{-\infty}^{\infty} \frac{e^{-j\alpha\sqrt{x^2+t^2}}}{\sqrt{x^2+t^2}}dt = -j\pi H_o^{(2)}(\alpha x), \tag{2-6}$$

the EFIE reduces to

$$\frac{k\eta}{4}\int_L J_z(\rho')H_o^{(2)}(kR)dl = E_z^i(\rho). \tag{2-7}$$

Here, L is the surface profile in the x-y plane, and $H_o^{(2)}(kR)$ is the zero order Hankel function of the second type. This equation is a scalar integral equation and is directly solvable by the moment method. Similarly, the surface current re-radiation reduces to

$$\mathbf{E}^s = -\hat{a}_z\frac{k\eta}{4}\int_L J_z(x')H_o^{(2)}(k|\rho-\rho'|)dx'. \tag{2-8}$$

The Magnetic Field Integral Equation

The magnetic field integral equation is used to describe scattering from a rough

surface at vertical polarization. The MFIE insures that the boundary condition

$$\mathbf{J}_s = \hat{a}_n \times (\mathbf{H}^s - \mathbf{H}^i) \tag{2-9}$$

is met, where $\mathbf{H}^s$ is the scattered magnetic field, and $\mathbf{H}^i$ is the incident magnetic field. For

a general 2-D scattering problem the MFIE is given by [Balanis 1989]

$$\frac{J_s(\mathbf{r})}{2} - \hat{a}_n \times \iint_{S-\Delta S} J_z(\mathbf{r}')G(\mathbf{r}, \mathbf{r}')ds' = \hat{a}_n \times H^i(\mathbf{r}). \tag{2-10}$$

The integration domain S-ΔS indicates the principal-value evaluation of the integral

around the singularity at $\mathbf{r} = \mathbf{r}'$. The MFIE is also a vector integral equation for the

surface current. Likewise, it can also be simplified for the two dimensional case. Using

the same arguments as in the last section and assuming a TM^z polarized incident wave,

equation 2-10 reduces to

$$\frac{J_s(\mathbf{r})}{2} + \frac{jk}{4}\int_{L-\Delta l} J_z(r')\cos\psi H_1^{(2)}(kR)dl' = -H_z^i(r) \tag{2-11}$$

This scalar integral equation is also solved by direct application of the moment method.

The scattered field is given by

$$\mathbf{H}^s(r) = -j\omega\mu \int_s J_s(\mathbf{r}')G(\mathbf{r}, \mathbf{r}')ds' + \frac{j}{\omega\epsilon}\nabla \int_s \nabla' \cdot J_s(\mathbf{r}')G(\mathbf{r}, \mathbf{r}')ds', \tag{2-12}$$

which for the two-dimensional case reduces to

$$H_z^s = \frac{jk}{4}\int_L J_s(\rho')\cos\psi H_1^{(2)}(kR)dl'. \tag{2-13}$$

where ψ is the angle between the distance vector and the normal vector at the observation

point.

The Moment Method

The moment method is used to approximate solutions to equations with the

general form [Harrington 1968]

$$L[f(\mathbf{R})] = g(\mathbf{R}), \tag{2-14}$$

9

L is an arbitrary linear integro-differential equation, f is an unknown function to be determined, and g is a known excitation function. In scattering problems, equation (2-14) corresponds to the MFIE or EFIE with $g(\mathbf{R})$ as the illuminating field (or source) and $f(\mathbf{R})$ is the unknown surface current.

The first step in applying the moment method is to approximate the unknown function as a weighted sum of N known basis functions:

$$f(\mathbf{R}) = \sum_{i=1}^{N} \alpha_i N_i(\mathbf{R}), \tag{2-15}$$

where $N_i(\mathbf{R})$ are the basis functions and α_i are unknown coefficients to be determined by the moment method. Substituting equation 2-15 into 2-14 and recalling the properties of a linear operator gives

$$\sum_{i=1}^{N} \alpha_i L[N_i(\mathbf{R})] = g(\mathbf{R}). \tag{2-16}$$

The residual of this approximate solution is

$$Res(\mathbf{R}) = \sum_{i=1}^{N} \alpha_i L[N_i(\mathbf{R})] - g(\mathbf{R}) \tag{2-17}$$

The values of the coefficients are chosen to minimize this residual.

The moment method uses the method of weighted residuals to find the optimal weighting coefficients. The weighted residuals are obtained by taking the inner product of the residual and N weighting functions $w_j(\mathbf{R})$. The inner product is defined by

$$<w_j(\mathbf{R}), Res(\mathbf{R}) > = \int_\Omega w_j(\mathbf{R}) Res(\mathbf{R}) d\Omega \tag{2-18}$$

Setting these weighted residuals to zero and again taking advantage of the linearity of the L operator gives the general moment equation:

$$\sum \alpha_i \int_\Omega w_j(\mathbf{R}) L[N_i(\mathbf{R})] d\Omega = \int_\Omega w_j(\mathbf{R}) g(\mathbf{R}) d\Omega \tag{2-19}$$

This equation has N linear algebraic equations and N unknowns, and can be readily solved for α_i using general linear algebra methods.

Examining equation (2-19), it is seen that the moment method is a two step process. The first step is to "fill" the moment interaction matrix. This step includes a numerical integration for each matrix element and increases processing time by N^2 as more basis functions are used to describe the surface. The second step is to solve the system of equations generated for the unknown coefficients, α_j's. The direct linear algebra methods usually used to solve for the α_j coefficients are order N^3. Because of this the solve time is usually the limiting factor in the standard moment method. However, the fill time is actually greater in the periodic surface implementation used here.

Basis Functions

The choices for basis functions are limitless. They can include either entire domain functions valid over the entire surface or sub-domain basis functions valid over only a portion of the surface [Harrington 1968]. Sub-domain basis functions are typically used for electromagnetic scattering problems. Traditional choices for sub-domain basis functions in electromagnetic scattering problems include pulse functions, piecewise sinusoid and piecewise linear functions [Balanis 1989]. The basis functions should be chosen , if possible, to closely approximate the unknown function while striving to minimize the computational effort expended.   The basis functions used in this work are subdomain pulse functions, as shown in Figure 2.2. With this method the surface is divided into a series of small segments and the current density along the segment is considered constant.

Figure 2.2 A Pulse Basis Function

Using this basis function produces a stairstep approximation to the surface current as

shown in Figure 2.3.

The pulse basis functions were chosen for their computational simplicity. The evaluation

of the linear operator in the EFIE and/or MFIE can be accurately evaluated without the

use of numerical integration [Harrington, 1968]. While fewer basis functions could

theoretically be used with "better" basis functions which more accurately approximate the

actual current density, in practice it has been shown that the actual reduction is small, and

any advantages are more than outweighed by the increased matrix fill time [Axline and

Fung 1978].

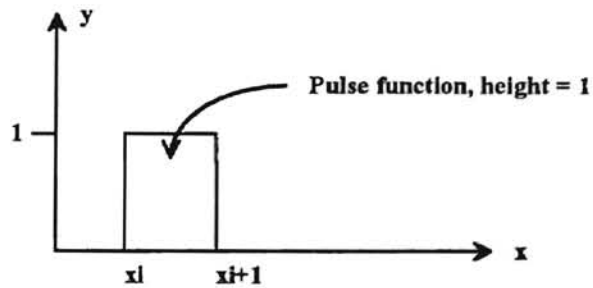**Figure 2.3 A Stairstep Current Approximation**

Figure 2.2 A Pulse Basis Function

Using this basis function produces a stairstep approximation to the surface current as

shown in Figure 2.3.

The pulse basis functions were chosen for their computational simplicity. The evaluation

of the linear operator in the EFIE and/or MFIE can be accurately evaluated without the

use of numerical integration [Harrington, 1968]. While fewer basis functions could

theoretically be used with "better" basis functions which more accurately approximate the

actual current density, in practice it has been shown that the actual reduction is small, and

any advantages are more than outweighed by the increased matrix fill time [Axline and
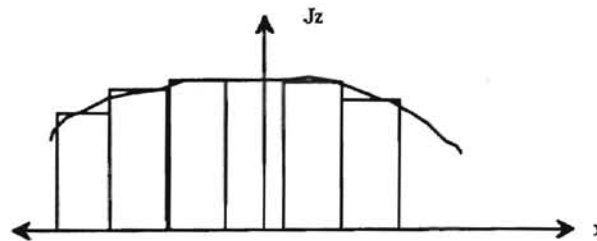
Fung 1978].

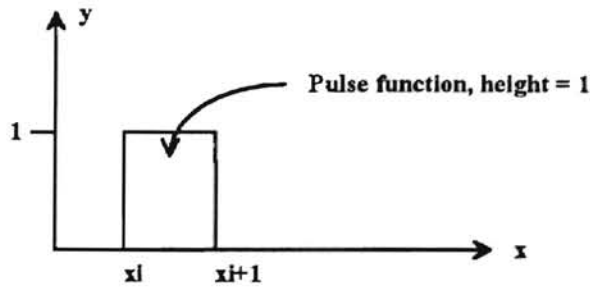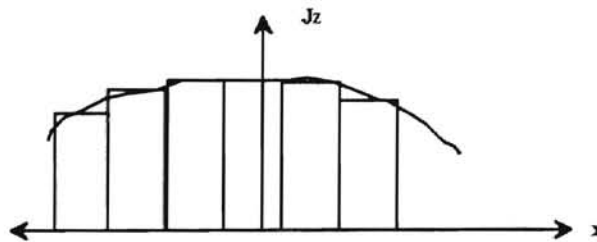**Figure 2.3 A Stairstep Current Approximation**

Weighting Functions

As with the basis functions, many choices are available for weighting functions. In this work the weighting functions are chosen to be Dirac delta functions,(or impulse functions) centered on the basis functions. This choice forces the surface boundary conditions to be matched exactly at the point of the impulse. The primary advantage of this approach is that the inner product in equation (2-18) reduces to the evaluation of the operand at discrete points, thus eliminating the integration entirely. Again, this has been shown to yield good results when applied to rough surface scattering [Chen and Fung].

Traditional MM Scattering

The moment method is now applied to the EFIE to yield the currents on a one-dimensional rough surface at horizontally polarized illumination. The EFIE in equation (2-7) is first rewritten as

$$E_z^i(x) = \frac{k\eta}{4} \int \sqrt{1 + h_x^2(x')}\, J_s(x') H_o^{(2)}(kR) dx', \tag{2-20}$$

where h(x') is the surface displacement and h_x(x') is the first derivative, with respect to x', of the displacement. The moment method is applied by expanding the unknown current as a weighted sum of pulse basis functions:

$$J_s(x') = \sum_{n=1}^{N} J_n P[x' - x_n], \tag{2-21}$$

where J_n are the unknown weighting coefficients,

$$P(x') = \left\{ \begin{array}{ll} 1 & x_n - \frac{\Delta x_n}{2} < x' < x_n + \frac{\Delta x_n}{2} \\ 0 & \text{elsewhere} \end{array} \right\}, \tag{2-22}$$

and x_n, and Δx_n are the center and length of the nth segment respectively. Substituting (2-21) into (2-20) gives

$$E_z^i(x) = \frac{k\eta}{4} \sum_{n=1}^{N} J_n \int_{\Delta x_n} \sqrt{1 + h_x^2(x')}\, H_o^{(2)}(kR) dx' \tag{2-23}$$

13

the impulse weighting functions are now applied:

$$\int_{-\infty}^{\infty} E_z^i(x)\delta(x-x_m)dx = \frac{k\eta}{4}\sum_{n=1}^{N} J_n\int_{\Delta x_n} \sqrt{1+h_x^2(x_m)} \int_{-\infty}^{\infty} H_o^{(2)}(kR)\delta(x-x_m)dxdx' \quad (2\text{-}24)$$

so

$$E_z^i(x_m) = \frac{k\eta}{4}\sum_{n=1}^{N} J_n\int_{\Delta x_n} \sqrt{1+h_x^2(x_m)} \, H_o^{(2)}(kR_m)dx' , \quad (2\text{-}25)$$

where $R_m = \sqrt{(x_m-x')^2 + [h'(x_m)-h(x')]^2}$.

Evaluating at the N segments, (2-25) can be rewritten as the matrix equation

$$[Z_{mn}][J_n] = [V_m] \quad (2\text{-}26)$$

where $V_m = E_z^i(x_m)$ and

$$Z_{mn} = \frac{k\eta}{4}\int_{\Delta x_n} \sqrt{1+h_x^2(x_m)} \, H_o^{(2)}(kR_m)dx' \quad (2\text{-}27)$$

Solving (2-26) for the J_n completes the moment method solution.

There is no closed form expression for the integral in equation (2-27), but if certain conditions are met there are good approximations[Harrington 1968]. If the integration length is electrically small and the observation point (x_m) is not on the nth segment, the integrand is approximately constant and (2-27) can be evaluated by

$$Z_{mn} = \frac{k\eta}{4}\Delta l_n H_o^{(2)}(kR_{mn}) \quad (2\text{-}28)$$

where

$$\Delta l_n = \sqrt{1+h_x^2(x_n)} \, \Delta x_n . \quad (2\text{-}29)$$

and

$$R_{mn} = \sqrt{(x_m-x_n')^2 + [h'(x_m)-h(x_n')]^2} \quad (2\text{-}30)$$

If the observation point is on the source segment, the integral is dominated by the behavior of the integrand at the singularity at $R_{mn} = 0$. In this case the equation (2-27) is accurately represented by

$$Z_{mm} = \frac{k\eta}{4}\Delta l_i H_o^{(2)}(1-j\frac{2}{\pi}\ln\frac{\gamma k\Delta l_m}{4e}) \quad (2\text{-}31)$$

where $\gamma = 1.781$, is the Euler constant.

Use of the magnetic field integral equation with the moment method and point matching is similar to this development with the EFIE [Axline and Fung, 1978].

14

The Periodic Surface Moment Method

Finite computer resources limit the size of the scattering surface that can be treated with the standard moment method. The number of segments used to model the surface increases linearly with the surface size, and the memory needed to store the interaction matrix increases by N^2. Also the computational time needed to solve the system of linear equations depends on N^3. Thus both the CPU time needed to solve the equations, and the memory needed to store the complex interaction matrix elements limit the size of the surface that can be solved with this method, so the numerically modeled surface must be artificially truncated. This truncation leads to non-physical edge diffraction effects that mask the physical scattering from the surface. The standard moment method avoids the diffraction by applying a weighting function that smoothly reduces the incident field to zero at the edges. However, Thorsos (1988) showed the electromagnetically valid weighting windows become quite narrow beams at small grazing angles, leading to unrealistic illumination of the surface features that gives incorrect scattering.

Many of the disadvantages of the standard moment method at small grazing angles can be overcome by assuming that the scattering surface is periodic and infinitely extending, as shown in Figure 2-4. Although only a finite length of surface is numerically modeled, the assumption of periodicity eliminates the edges. Thus, no illumination weighting function is needed to avoid the diffraction effects, so the technique can be applied at arbitrarily small grazing angles [Kim et. al., 1992]. The primary disadvantage of this approach is that a slowly converging infinite series must be evaluated during the fill
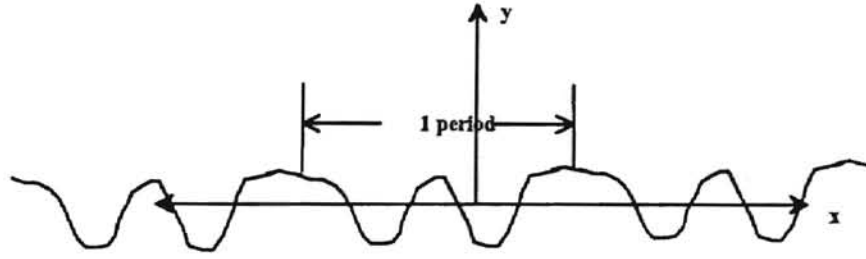
Figure 2.4 A Surface Made Periodic

stage of the moment solution. Direct evaluation of the series is computationally

prohibitive at small grazing angles.

In this work the efficient implementation of the periodic surface moment method

developed by Chen and West (1995) is used. This approach is summarized here.

Horizontal Polarization

As mentioned earlier, the electric field integral equation is used for horizontal

polarization(HH). The current on the periodic surface is given by

$$J(x' + pL) = e^{jkpL \sin \theta_i} J(x').$$ (2-32)

The form of the EFIE for periodic surfaces is obtained by substituting (2-32) into (2-8),

yielding

$$E_o(x) = \frac{k\eta}{4} \int_{-L/2}^{L/2} \sqrt{1 + h_x^2(x')} \, J(x') \sum_{p=-\infty}^{p=\infty} e^{jkpL \sin \theta_i} H_o^{(2)}(kR_p) dx'$$ (2-33)

J(x') is the unknown current density on the center period (p = 0), θ_i is the incident angle,

L is the surface period, and R_p is the distance from the current source to the observation

point given by

$$R_p = \sqrt{[x - (x' + pL)]^2 + [h(x) - h(x')]^2}$$ (2-34)

16

The moment method is applied as before, yielding

$$
Z_{mn}^h = \frac{k\eta}{4}\Delta \ln \left\{ \begin{array}{ll} \displaystyle\sum_{p=-\infty}^{p=\infty} e^{jkpL\sin\theta_i} H_o^{(2)}(kR_{mnp}) & m \neq n \\[2mm] [1-j\frac{2}{\pi}\ln(\frac{\gamma k\Delta l_n}{4e}) + \displaystyle\sum_{p=-\infty}^{p=\infty} e^{jkpL\sin\theta_i} H_o^{(2)}(kR_{mnp}) & m=n \end{array} \right\}
$$

(2-35)

where $R_{mnp} = \sqrt{[x_m - (x_n + pL)]^2 + [h(x_m) - h(x_n)]^2}$ and Δl_n is defined earlier.

The matrix elements include an infinite series that has no closed form evaluation. At lower incident angles the series converges quickly and only a few terms are needed to obtain accurate results. However, as the angle of incidence increases towards grazing angles the series converges more and more slowly, and as the incidence angle approaches 90° direct evaluation of the series becomes quite time consuming. Thus, the matrix fill time becomes prohibitive at large incidence angles if direct evaluation is used.

In Chen and West's approach, the matrix element equation is rewritten as

$$
Z_{mn}^h = \frac{k\eta}{4}\Delta l_n [s_{mn}^{h+} + s_{mn}^{h-} + s_{mn}^{ho}],
$$

(2-36)

where

$$
S_{mn}^{h+} = \sum_{p=p_o+1}^{\infty} e^{jkpL\sin\theta_i} H_o^{(2)}(kR_{mnp}),
$$

(2-37)

$$
S_{mn}^{h-} = \sum_{p=-\infty}^{-p_o-1} e^{jkpL\sin\theta_i} H_o^{(2)}(kR_{mnp}),
$$

(2-38)

$$
S_{mn}^{h0} = \left\{ \begin{array}{ll} \displaystyle\sum_{p=-p_o}^{p=+p_o} e^{jkpL\sin\theta_i} H_o^{(2)}(kR_{mnp}) & m \neq n \\[2mm] [1-j\frac{2}{\pi}\ln(\frac{\gamma k\Delta l_n}{4e}) + \displaystyle\sum_{p=-p_o,p\neq0}^{p=p_o} e^{jkpL\sin\theta_i} H_o^{(2)}(kR_{mnp}) & m=n \end{array} \right\},
$$

(2-39)

Thus, the infinite series has been divided into an upper (h⁺), lower (h⁻), and center (h⁰) summation. Proper choice of the cutoff period (p_o) insures that all effects of the surface displacements are included in the evaluation of the S_{mn}^{h0}. This sub-series must therefore be evaluated exactly for each matrix element. However, the lower and upper summations can be calculated much more efficiently. The upper series is examined first.

When the source point is a great distance from the observation point the distance between them can be approximated by

$$R_{mnp} \approx pL + \delta x, \quad p > 0 \tag{2-40}$$

where, $\delta x = x_n - x_m$. Substituting (2-37) into (2-35), replacing the Hankel function with its large argument approximation and performing a Q order Taylor expansion gives

$$S_{mn}^{h+} = \sqrt{\frac{2}{\pi k}} \, e^{-j(k\delta x - \frac{\pi}{4})} \sum_{q=0}^{Q} (-1)^q A_q U_q^+ \delta x^q, \tag{2-41}$$

where

$$U_q^+ = \sum_{p=p_o+1}^{\infty} e^{-jkpL(1-\sin \theta_i)} \frac{1}{(pL)^{q+\frac{1}{2}}}, \tag{2-42}$$

and

$$A_q = \frac{(2q-1)!!}{(2q)!!} \tag{2-43}$$

These same arguments can be used to reduce equation 2-40, the lower summation, to

$$S_{mn}^{h-} = \sqrt{\frac{2}{\pi k}} \, e^{j(k\delta x + \frac{\pi}{4})} \sum_{q=0}^{Q} A_q U_q^- \delta x^q \tag{2-44}$$

where

$$U_q^- = \sum_{p=p_o+1}^{\infty} e^{-jkpL(1+\sin \theta_i)} \frac{1}{(pL)^{q+\frac{1}{2}}} \tag{2-45}$$

The evaluation of both the upper and lower summations have been reduced to evaluating a linear combination of the upper and lower "universal series" U_q^+ and U_q^-. All dependencies on m and n are contained solely in δx. For this reason the universal series for each matrix element are identical and need only be evaluated a single time. This approach reduces the calculation of the moment interaction matrix to evaluating the universal series once and combining with it a few direct calculations for each elements' center summation. This greatly improves the efficiency of evaluating the matrix terms.

18

Vertical Polarization

The vertical polarization development of the universal summation approach to the periodic-surface moment method is similar to that taken for the horizontal polarization, except the magnetic field integral equation is now used. The MFIE for uniform illumination and a periodic surface reduces to [Kim et. al 1992].

$$-Hi(x) = \frac{J(x)}{2} + \frac{jk}{4} \int_{-L/2}^{L/2} \sqrt{1+h_x^2(x')}\, J(x') \sum_{p=-\infty}^{\infty} e^{jkpL\sin\theta_i} \cos\psi' H_1^{(2)}(kR_p)\,dx', \qquad (2\text{-}46)$$

where ψ' is the angle between the vector from the source to observation point and the surface normal vector at the source point. Following a similar procedure as that for the EFIE yields,

$$Z_{mn}^{v} = \tfrac{1}{2}\delta_{mn} + \Delta l_n \tfrac{jk}{4}(S_{mn}^{v+} + S_{mn}^{v-} + S_{mn}^{v0}) \qquad (2\text{-}47)$$

where

$$\delta_{mn} = \text{the Kronecker delta function} = \begin{Bmatrix} 1\ for\ m=n \\ 0\ for\ m \neq n \end{Bmatrix}, \qquad (2\text{-}48)$$

$$S_{mn}^{v+} = \cos\psi_n' \sqrt{\frac{2}{\pi k}}\, e^{-j(k\delta x - \frac{3\pi}{4})} \sum_{q=0}^{Q} (-1)^q A_q U_q^+ \delta x^q, \qquad (2\text{-}49)$$

$$S_{mn}^{v-} = \cos\psi_n' \sqrt{\frac{2}{\pi k}}\, e^{j(k\delta x + \frac{3\pi}{4})} \sum_{q=0}^{Q} A_q U_q^- \delta x^q, \qquad (2\text{-}50)$$

$$S_{mn}^{v0} = \begin{Bmatrix} \sum_{p=-P_o}^{P_o} \cos\Psi_{mnp}' e^{jkpL\sin\theta_i} H_1^{(2)}(kR_{mnp}) & m \neq n \\ \sum_{p=-P_o,p\neq 0}^{P_o} \cos\Psi_{mnp}' e^{jkpL\sin\theta_i} H_1^{(2)}(kR_{mnp}) & m = n \end{Bmatrix} \qquad (2\text{-}51)$$

U_q^+ and U_q^-, are the universal series defined earlier and

$$\cos\psi_{mnp}' = \frac{[x_n - x_m + pL]h_x(x_n) + [h(x_m) - h(x_n)]}{R_{mnp}\sqrt{1+h_x^2(x_n)}}, \qquad (2\text{-}52)$$

$$\cos\psi_n' = -\frac{h_x(x_n)}{\sqrt{1+h_x^2}} \qquad (2\text{-}53)$$

The evaluation of matrix elements has again been reduced to evaluating each universal series once and the direct evaluation of a few center terms.

Scattering Calculations

The moment method yields the current induced on the scattering surface by the incident field. The re-radiation of the surface current is then used to find the scattered field from which the surface radar cross-section is determined. The radar scattering coefficient of a surface is defined as the radar cross section of a surface divided by its physical cross section. This work uses one dimensionally rough surfaces, so the scattering coefficient calculations are therefore referenced to the surface length rather than an area. In order to reduce the phase interference fading encountered when calculating the backscattering from a single surface, the scattering from N_s surfaces is averaged. The one-dimensional surface scattering coefficient is estimated by [Axline and Fung, 1982]

$$\sigma(\theta) = \frac{2\pi R}{N_s L}\left[\sum_{j=1}^{N}\left|A_j^s\right|^2 - \frac{1}{N_s}\left|\sum_{j=1}^{N}A_j^s\right|^2\right] \tag{2-54}$$

where A_j^s is the scattered field from the jth surface, R is the distance from the far field observation point to the to the source point, and L is the length of the scattering surface. At horizontal polarization, A_z^s is the electric field scattered from a single surface period, given by [Axline and Fung, 1982; Chen and West, 1995].

$$E_z^s = \eta\sqrt{\frac{k}{8\pi r}}\,e^{-j(kr+\frac{3\pi}{4})}\sum_{p=-\infty}^{\infty}e^{jkpL(\sin\theta_i+\sin\theta_s)} \tag{2-55}$$

where θ_s is the scattering angle.

At vertical polarization A_z^s is the single-period scattered magnetic field given by

$$\sqrt{\frac{k}{8\pi r}}\,e^{-j(kr+\frac{3\pi}{4})}\sum_{n=1}^{N}\Delta l_n J(x_n)\cos\Psi_n e^{jk[x_n\sin\theta_i+h(x_n)\cos\theta_i]}dx \tag{2-56}$$

Parameter Constraints

Chen and West derived several constraints on the parameters of the periodic surface required for the validity of the moment method solution. These are now summarized.

20

The scattering from a periodic surface is zero everywhere except on a grating

re-radiation lobe, defined when

$$\sin\theta_s = \frac{s\lambda}{L} - \sin\theta_i .$$
(2-57)

If a grating lobe exists at ±90° (horizontal), the infinite series in the periodic surface EFIE

and MFIE do not converge. This can be avoided by insuring

$$L \neq \frac{t\lambda}{\sin\theta_i \pm 1}$$
(2-58)

where t is any integer.

Approximations made in deriving equation (2-41), (2-44), (2-49), and (2-51)

require the following inequalities to be met:

$$P_o > \frac{10}{kL},$$
(2-59)

$$P_o > \frac{8(h_{max}-h_{min})^2}{L\lambda},$$
(2-60)

$$P_o > \frac{22.4(h_{max}-h_{min})}{L}$$
(2-61)

where h_{max} = the maximum displacement of the surface, and h_{min} is the minimum

displacement.

Universal Series Evaluation

When the incidence angle nears 90° the universal series converge very slowly and

direct evaluation becomes computationally prohibitive. The epsilon algorithm for

acceleration of series convergence was therefore applied to the universal series with

excellent results [Thatcher 1963].

Approximate Scattering Theories

The two most popular approximate rough surface scattering theories are the Kirchoff approximation (KA) and the small perturbation model (SPM). A brief summary of these theories is given here.

The Kirchoff Approximation

The Kirchoff approximation assumes that the current induced on the scatterer surface can be approximated by treating the local region of the surface as an infinite, perfectly conducting inclined plane [Beckman and Spizzichino, 1963]. Using this, the surface current is then determined from the physical optics approximation:

$$\mathbf{J}_s = 2\hat{\mathbf{a}}_n \times \mathbf{H}^i \tag{2-62}$$

The KA is valid with electromagnetically long correlation-length surfaces or large-scale displacement surfaces at moderate incidence angles. The scattering coefficients predicted by the Kirchoff approximation were determined using the approach of Chen and Fung (1988). In this, the scattering coefficient is again calculated using equation (2-54). However, the scattered fields are calculated from the physical optics currents numerically determined from equation (2-62) rather than the surface currents obtained via the moment method. Use of this approach insures that any differences in the calculated MM and KA scattering coefficients will be due to fundamental limitations of the Kirchoff approximation itself, rather than the additional approximations required to yield a closed form KA expression as in Beckman and Spizzichino (1963).

The Small Perturbation Model

The small perturbation method finds the total field in the presence of a smooth scatterer, and then perturbs these fields to account for the small-scale roughness. First order SPM predicts the scattering to be entirely due to the "Bragg-resonant" surface wave energy, whose wave number is given by

$$K = 2k \sin \theta_i \qquad (2\text{-}63)$$

where K is the surface wave number. When this condition is met, the additional round trip electrical path length between identical points on the surface wave but within different periods is an integer multiple of the radar wavelength i.e. $2\Delta R \sin \theta_i = n\lambda$, as shown in Figure 2.5. This yields constructive interference which overwhelms all other scattering contributions. The scattering coefficients predicted by first order SPM (n=1) are

$$\sigma_{vv} = 4K^3(1 + \sin^2(\theta))W(2K\sin(\theta)) \qquad (2\text{-}64)$$
$$\sigma_{hh} = 4K^3\cos^4(\theta)(W(2K\sin(\theta))) \qquad (2\text{-}65)$$

where W(K) is the surface roughness power spectral density. W(k) will be estimated from the sample surface displacements to allow the calculation of the scattering coefficients using SPM.
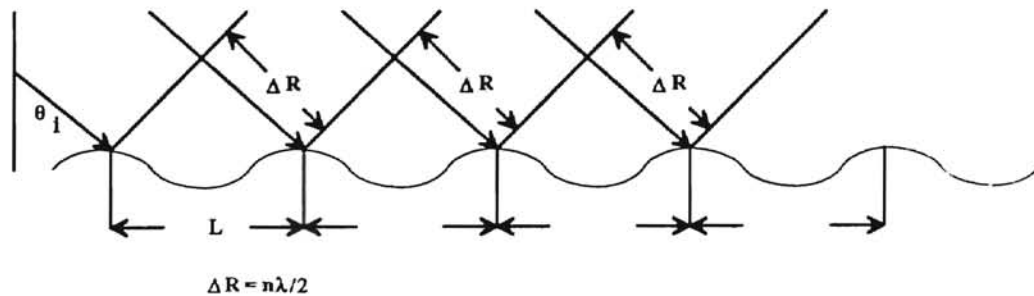

$$\Delta R = n\lambda/2$$

Figure 2.5 Mechanism for Bragg-Resonance Scattering

Chen and Fung (1988) have shown the small perturbation model to be accurate when the surface roughness standard deviation is small compared to the electromagnetic wavelength and angle of incidence is between about 20° and 70°.

CHAPTER 3

THE SURFACES AND THEIR PREPARATION

Introduction

This chapter discusses the measurement and processing of the water surface profiles that were used in the electromagnetic scattering calculations. Surface slope profiles measured in a wave tank were provided by B. Jahne and J. Klinke of Scripps Institute of Oceanography. The measurement facilities and measurement procedure are first discussed in this chapter. Then the procedure used to derive the surface displacement profile from the slope is described, and the adjustments to the surface required to allow the application of the periodic surface moment method are then examined. Finally, the procedure used to estimate the wave height spectrum from the surface profiles is described.

The Data Collection

The wave tank data used was collected from a circular wave tank facility at the Institute for Environmental Physics at the University of Heidleburg, Germany [Jahne and Klinke, 1994]. The apparatus used for this data collection is depicted in Figure 3.1.
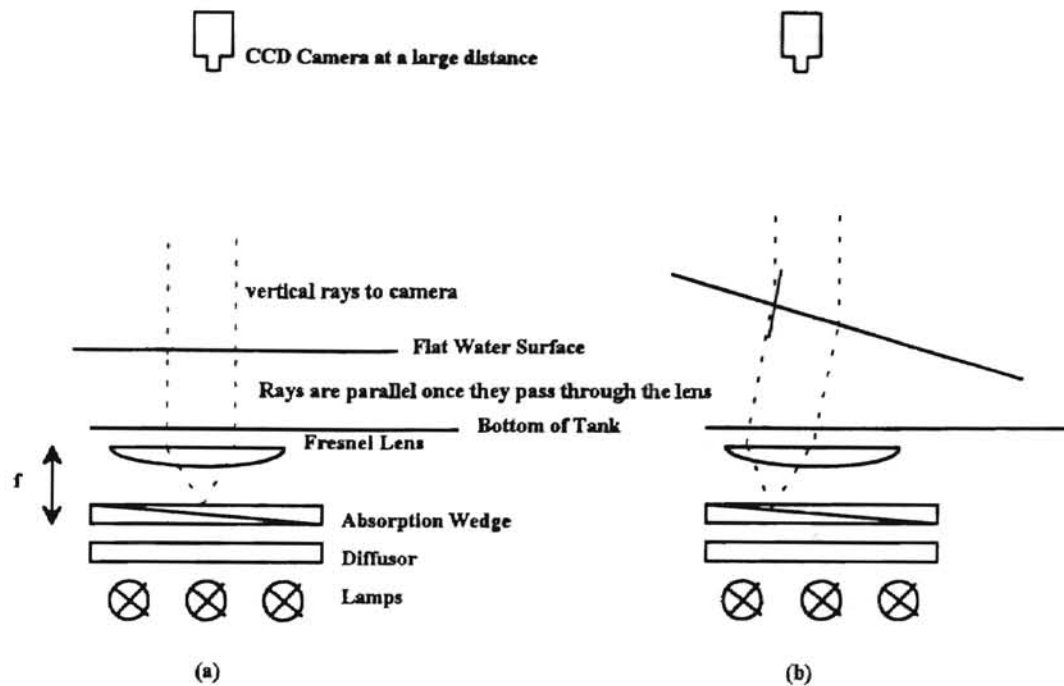
Figure 3.1 The Apparatus Used to Measure Slope Data

This particular setup shines light from the under the bottom of the wave tank up through the combination of an optical diffusor, an absortpion wedge, and a Fresnel lens at one focal length distance from the wedge. A ccd camera is placed at a large distance, therefore all rays reaching the camera are vertical. The optical diffusor is meant to simulate an isotropic light source by diffusing the light from the halogen lamps below. The absorptive wedge provides a known intensity gradient. The light then passes to the Fresnel lens, all rays emitted from a certain point on the diffusor are parallel once they pass through the lens. If the water is flat the rays going to the camera will all come from the center of the diffusor as shown in Figure 3-1a. If the water is sloped the light comes
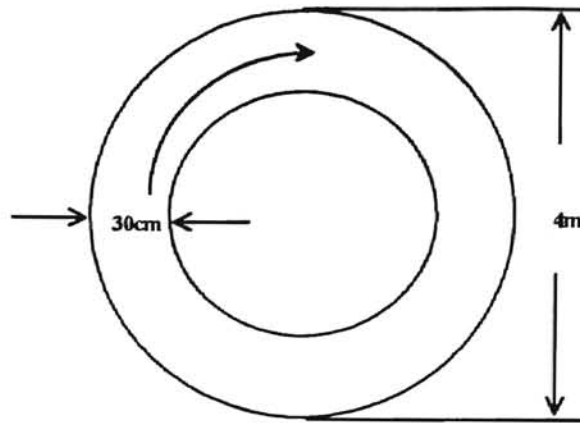
26

Figure 3.2 The Circular Wave Tank

from another point on the diffusor as shown in Figure 3-1b. If a linear absorption wedge

is used, the intensity at the camera is approximately linearly related to the slope. Jahne

and Schultz (1992) showed that the non-linearities for the system used here are quite low.

The Samples

The wave-tank data provided was captured from a circular wave tank as pictured

in Figure 3.2. The wind was generated by a rotating paddle wheel mounted near the

ceiling of the water channel. The speed of the wind driving the waves was 10 meters per

second and the fetch of the waves produced is theoretically infinite [Jahne and Klinke

1994], mimicking the conditions in the open sea.

An image of a patch of the surface 18cm long in the along-wind direction and

14cm in the across wind direction was provided. The along wind dimension was sampled
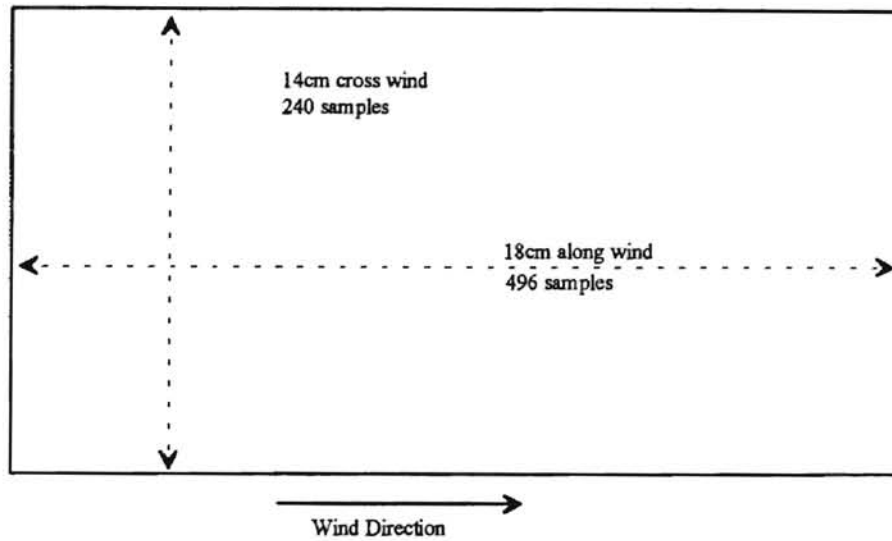
Figure 3.3 Surface Patch Dimension

496 times, while the cross wind dimension was sampled 240 times, giving along wind and

across wind sampling intervals of 0.363 and 0.583 millimeters respectively. Since only

one dimensional surfaces can be treated with the moment method implementation of

chapter two, each of the 240 along wind slices was processed separately and scattering

from each was used for the backscattering coefficient calculations. Due to correlation

between adjacent alongwind slices, the number of independent surfaces is much less than

240, as discussed later.

Data Processing

Figure 3.4 shows a single along-wind slice of the surface slope profile. The

discontinuity of 2.198355 when the slopes exceeded 1.0991775 is most likely due to an
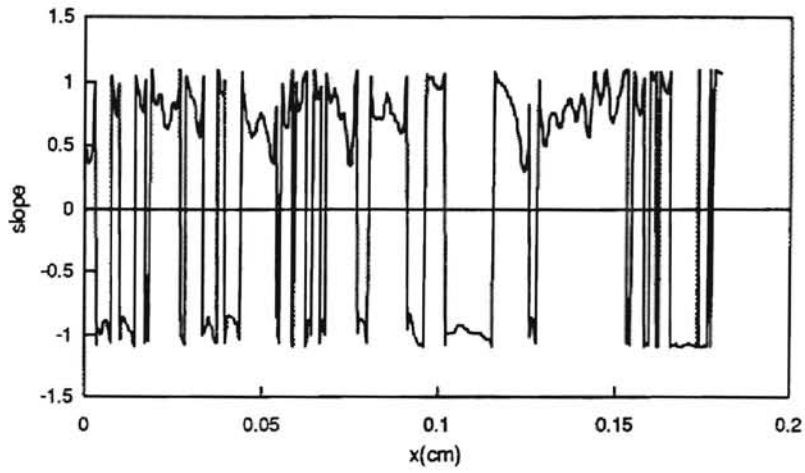
28

Figure 3.4 A Slice of pre-processed slope data

unsigned integer being treated as a signed integer in the data writing or reading scheme.

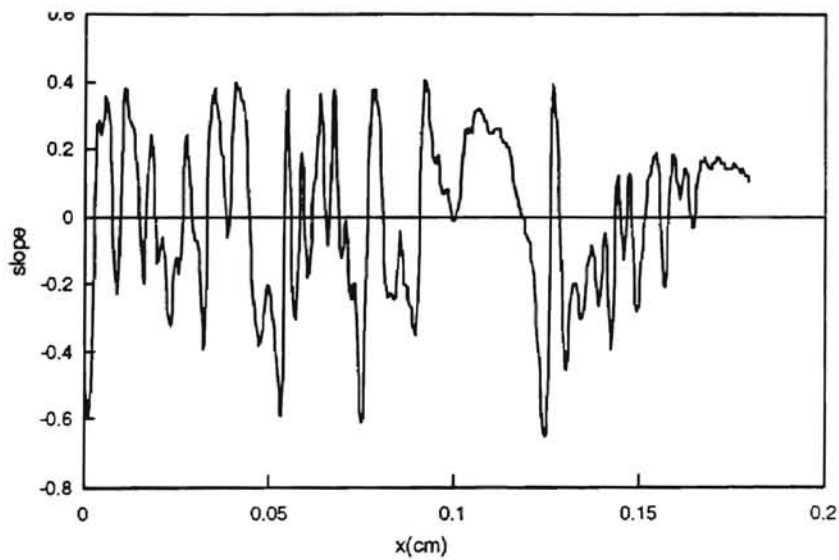The discontinuities and mean offset were removed, as shown in Figure 3.5.

Figure 3.5 Zero Mean Slope Data

29

Surface Displacement

The moment method requires the surface displacement as well as the surface slope. This was obtained by numerically integrating the slope profile. The displacement at the nth sample was given by

$$y_{n+1} = y_n \delta x + y_n \qquad (3\text{-}1)$$

where y'_n is the is the surface slope at the nth sample and δx is the along-wind sampling interval. The integration was initialized by setting $y_o = 0$.

The numerical scattering routine requires the rough surface to be periodic. Simply assuming the integrated profile is periodic would lead to discontinuities in the surface slope as shown in Figure 3.6. Note that there is no discontinuity in the height since the average slope was forced to be zero, giving a zero displacement at both ends of the surface profile. However, the slope discontinuity gives a sharp edge in the surface that could lead to unrealistic scattering particularly at the higher frequencies examined.
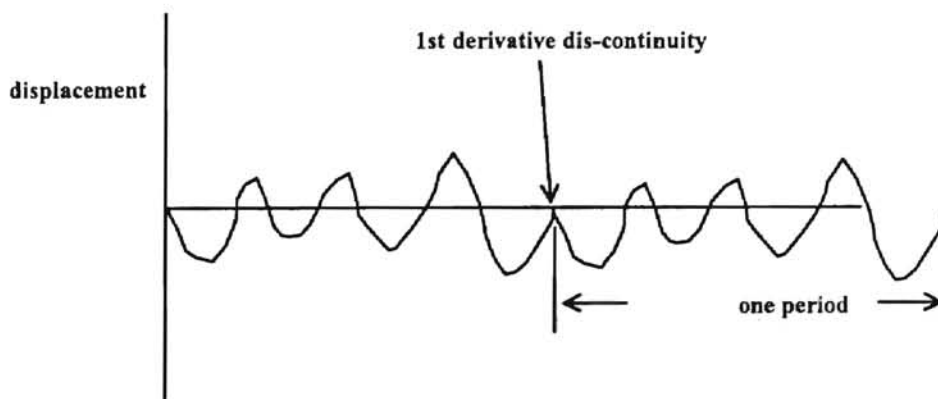

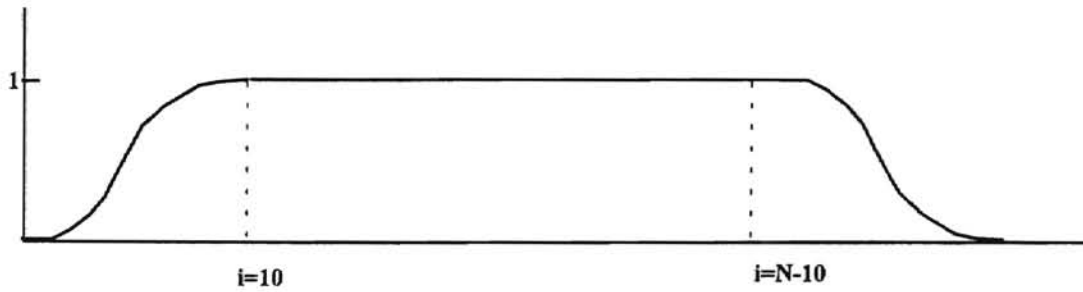**Figure 3.6 A Period Boundary Dis-Continuity**

Figure 3.7 The Raised Cosine Window

This was avoided by multiplying the height profile with the windowing function shown in

Figure 3.7. Each edge of the window represents one half cycle of a raised cosine function,

The weighting function is written mathematically as

$$W(x) = \begin{cases} \frac{1}{2}(1 - \cos\frac{x}{\Delta x}\pi) & 0 \leq x \leq \Delta x \\ \frac{1}{2}(1 - \cos\frac{x_{max}-x}{\Delta x}\pi) & \Delta x \leq x \leq x_{max} - \Delta x \\ 1 & elsewhere \end{cases} . \tag{3-2}$$

where $\Delta x = \frac{0.18m}{496}$, the along wind sampling distance.

Δx was chosen to be $10\delta x$, so that 10 samples were modified on each side of the profile

(20 of the 496 total). Since the height data was changed by the window, the slope
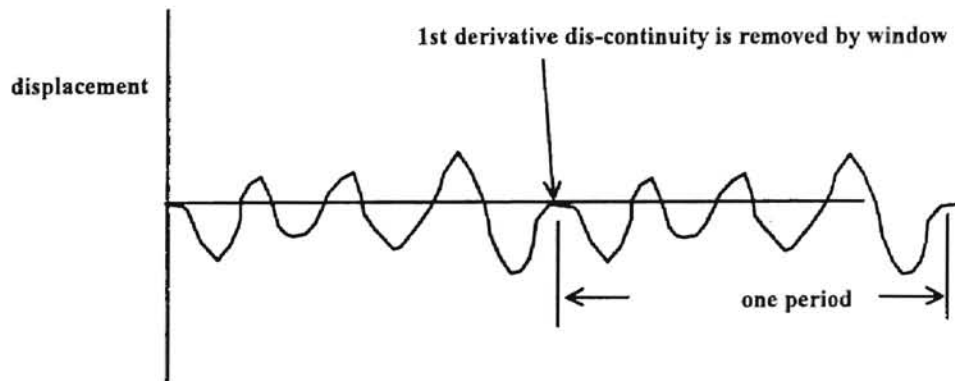
changed also.

Figure 3.8 Removing the Period Boundary Edges

31

The slope at the boundaries was re-calculated using the chain rule. The windowed height data is given by

$$h(x) = W(x)h(x),\qquad(3\text{-}3)$$

so the windowed slope data is

$$h'(x) = \frac{d}{dx}[W(x)h(x)] = W(x)h'(x) + W'(x)h(x).\qquad(3\text{-}4)$$

h'(x) is the slope profile.

Independent Profiles

As mentioned earlier, since the along-wind profiles were taken from the same image, adjacent profiles are not independent. To estimate the number of independent profiles available, the surface autocorrelation in the cross-wind direction was estimated.
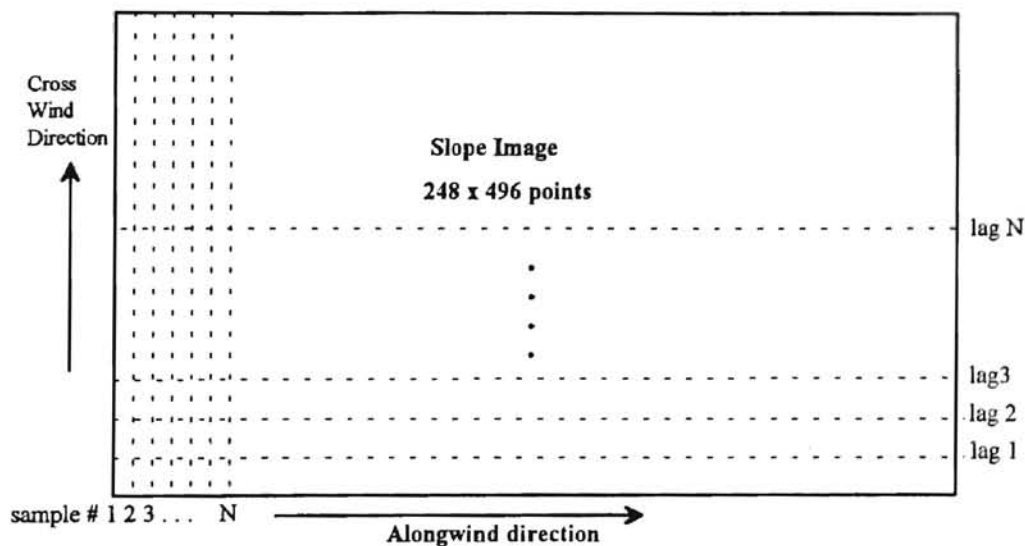

Figure 3.9 Slices used for Generating Surface Statistics

This was accomplished by calculating the autocorrelation function for a single cross-wind cut, shown in Figure 3.9, using

$$R(n) = \frac{1}{N-n} \Sigma_{m=n}^{N-n} h_k h_{k-n}, \qquad (3\text{-}7)$$

where h_k is the kth cross-wind displacement sample. The autocorrelation functions calculated for all 240 across-wind cuts were then averaged to give the estimated across-wind autocorrelation for the entire surface. The results are shown plotted in Figure 3.10.

The surface autocorrelation reduces to one half at approximately at $n = 7$ in Figure 3.10. The correlation of 0.5 is used in conjunction with the widely accepted 3-dB antenna beamwidth to indicate uncorrelation between samples [Ulaby, et. al. 1982]. Thus, there are approximately $\frac{248}{7}$ or 35 independent surfaces in the image. The normalized standard deviation of the calculated scattering coefficients are therefore $\frac{1}{\sqrt{35}} = 0.17$ [Ulaby, et. al.1982] giving an RMS error in the scattering coefficients of ± 0.7dB.
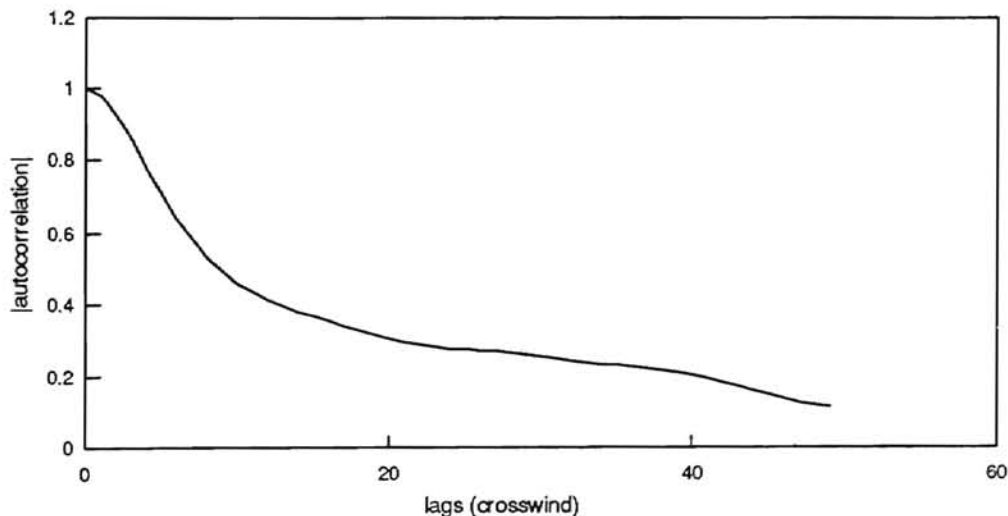

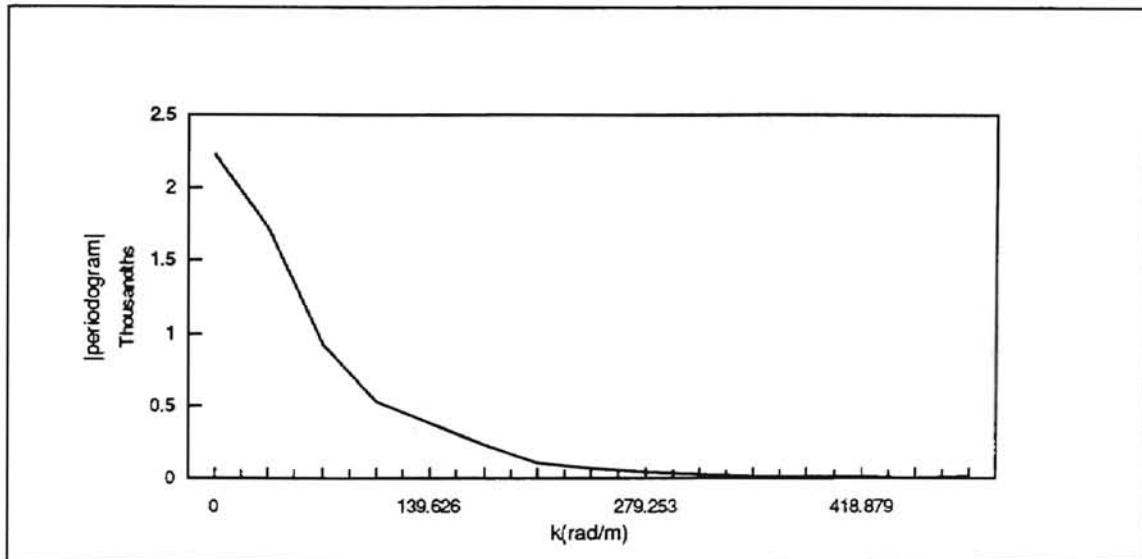**Figure 3.10 The Crosswind Autocorrelation Function**

Figure 3.11 Roughness Spectrum Estimate

Spectral Estimation

The surface power spectral density used in the small-perturbation scattering calculations was estimated using the periodogram calculated from the independent upwind surface profiles

[Bendat and Piersol, 1984]. The 496 point upwind slices of the surface profile were extended to 1024 points by zero padding and converted to the frequency domain using an FFT. The individual spectral lines were then squared and normalized to the number of points in the FFT (1024). The spectral lines at a given wave number were then averaged across the independent surfaces to yield the final spectral estimate. Again because approximately 35 independent surfaces were used the RMS error in the spectral estimate is about $\pm$ 17% ($\pm$0.7dB). Figure 3.11 shows the calculated periodogram. And Figure 3.12 shows the dB plot of the periodogram, along with the plots of several power-law spectra from k^{-3} to k^{-4} dependencies.

34

As mentioned before, the power law spectrum is an estimate of the saturated range of the power spectral density for the ocean surface. It has the form

$$W(k) = W_o k^{-\alpha} \qquad (3\text{-}8)$$

values of α ranging from 3 to 4 have been proposed. Expressing (3-8) in dB yields

$$10 \log_{10}(W(k)) = -10\alpha \log_{10}(k) + 10 \log_{10}(W_o). \qquad (3\text{-}9)$$

.Figure 3.12 shows that a = 3.5 gives a good prediction of the measured power spectral density in the saturated (high wave number) range.

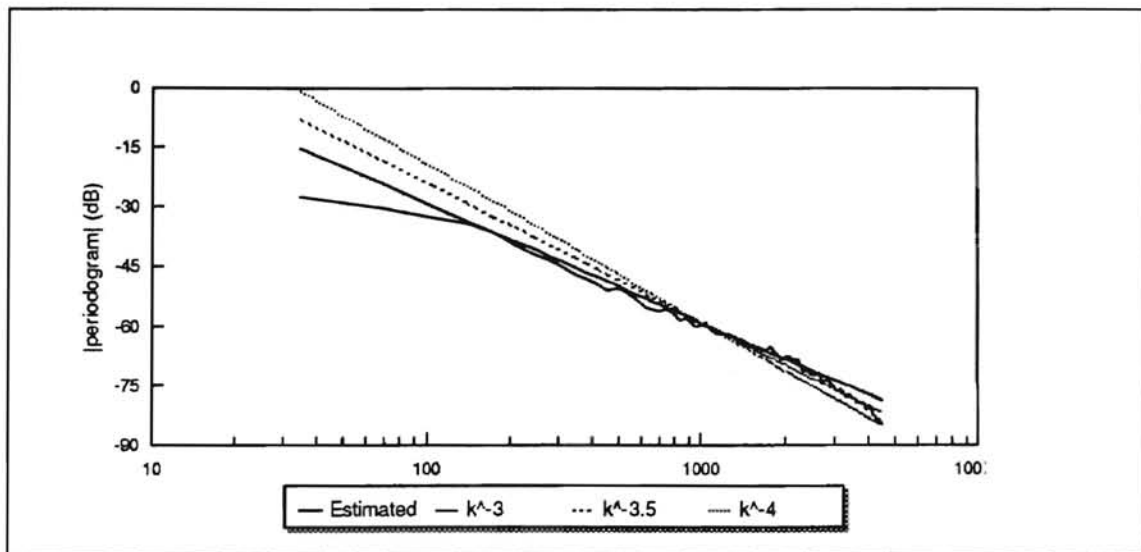Figure 3.12 dB Plot of Periodogram Estimate

CHAPTER 4

THE RESULTS OBTAINED WITH

EACH SCATTERING METHOD

INTRODUCTION

The scattering from the processed surfaces was calculated at frequencies ranging

from 8GHz to 58GHz and incidence angles ranging from 5° to 89°. This frequency range

was selected to test the validity of the small perturbation and Kirchoff approximation

scattering theories for different levels of surface roughness. As the frequency increases

the illumination wavelength decreases, and the surface displacements become electrically

larger. The results from the periodic surface moment method , small perturbation, and

Kirchoff theoretical scattering models, are compared at both horizontal and vertical

polarizations in this section.

Moment Method Parameters

Several physical parameters of the surface had to be varied with the frequency and

incidence angle in order to meet the conditions summarized in chapter two. In particular,

the length of the scattering surface was truncated from the full 18 cm to meet equations

(2-57) and (2-58). The number of terms in the infinite series of equations (2-35) and

(2-46) that were exactly evaluated was automatically determined from equations (2-59),

(2-61) and (2-62).

The number of basis functions used in the moment method description of the

surface was changed with frequency. Axline and Fung, (1978). showed that

approximately 10 basis functions are required per wavelength along the modeled surface

to yield an accurate MM prediction of the scattering. Use of more basis functions would

result in unneeded computational expense, while use of fewer would yield to inaccurate

results. Once the length and corresponding number of basis functions were calculated, the

height profile was re-sampled from a cubic spline fit of the surface. This resampled data

was used in the periodic surface calculations. The actual lengths of the modeled surface

used at each frequency and the associated numbers of basis functions are shown in table

4.1. Note that fewer basis functions are used as frequency decreases due to the longer

wavelength. Chen and West showed that a surface length of 5 wavelengths (50 basis

functions) is sufficient for accurate results at up to 89 degrees.

Results

Figures 4.1 through 4.6 show the calculated surface backscattering coefficient with

both horizontally and vertically polarized illumination at frequencies ranging from 8GHz

to 58GHz. The scattering coefficients calculated using the periodic surface moment

method, small perturbation model, and the Kirchoff approximation are shown. The RMS

surface heights, expressed in wavelengths, corresponding to each frequency used are

summarized in table 4.2.

Table 4.1 Parameters Used for Moment Method Analysis

Frequency	8GHz	18GHz	28GHz	38GHz	48GHz	58GHz
θ_1	L(m) and N	L(m) and N	L(m) and N	L(m) and N	L(m) and N	L(m) and N
5	0.22m 70 segments	0.19m 139 segments	0.19m 208 segments	0.18m 277 segments	0.2m 381 segments	0.19m 450 segments
10	0.22m 71 segments	0.19m 141 segments	0.19m 211 segments	0.18m 281 segments	0.18m 351 segments	0.18m 422 segments
15	0.19m 60 segments	0.18m 132 segments	0.18m 204 segments	0.18m 276 segments	0.18m 348 segments	0.18m 423 segments
20	0.2m 66 segments	0.18m 131 segments	0.18m 206 segments	0.18m 281 segments	0.18m 355 segments	0.18m 421 segments
25	0.2m 63 segments	0.18m 134 segments	0.18m 204 segments	0.18m 275 segments	0.18m 353 segments	0.18m 422 segments
30	0.19m 63 segments	0.18m 132 segments	0.19m 208 segments	0.18m 278 segments	0.18m 347 segments	0.18m 423 segments
35	0.2m 64 segments	0.19m 135 segments	0.18m 205 segments	0.18m 275 segments	0.18m 352 segments	0.18m 422 segments
40	0.19m 61 segments	0.19m 135 segments	0.18m 208 segments	0.18m 275 segments	0.18m 348 segments	0.18m 421 segments
50	0.19m 61 segments	0.19m 135 segments	0.18m 208 segments	0.18m 275 segments	0.18m 348 segments	0.18m 423 segments
60	0.19m 63 segments	0.18m 132 segments	0.19m 208 segments	0.18m 278 segments	0.18m 347 segments	0.18m 423 segments
65	0.2m 63 segments	0.18m 134 segments	0.18m 204 segments	0.18m 275 segments	0.18m 353 segments	0.18m 423 segments
70	0.2m 66 segments	0.18m 131 segments	0.18m 206 segments	0.18m 281 segments	0.18m 355 segments	0.18m 421 segments
75	0.19m 60 segments	0.18m 132 segments	0.18m 204 segments	0.18m 277 segments	0.18m 348 segments	0.18m 420 segments
78	0.18m 60 segments	0.18m 133 segments	0.18m 207 segments	0.18m 281 segments	0.18m 355 segments	0.18m 426 segments
80	0.22m 71 segments	0.19m 141 segments	0.19m 211 segments	0.18m 281 segments	0.18m 351 segments	0.18m 422 segments
82	0.2m 66 segments	0.18m 131 segments	0.19m 218 segments	0.19m 283 segments	0.18m 349 segments	0.19m 436 segments

38

Table 4.1 (cont)

85	0.22m	0.19m	0.19m	0.18m	0.2m	0.19m
	70 segments	139 segments	208 segments	277 segments	381 segments	450 segments
87	0.36m	0.24m	0.21m	0.19m	0.21m	0.2m
	115 segments	173 segments	230 segments	288 segments	402 segments	460 segments
88	0.27m	0.24m	0.23m	0.23m	0.22m	0.19m
	87 segments	173 segments	259 segments	345 segments	431 segments	431 segments
89	0.54m	0.24m	0.31m	0.23m	0.27m	0.22m
	172 segments	172 segments	344 segments	344 segments	516 segments	516 segments

Table 4.2 RMS Surface Height in Wavelengths

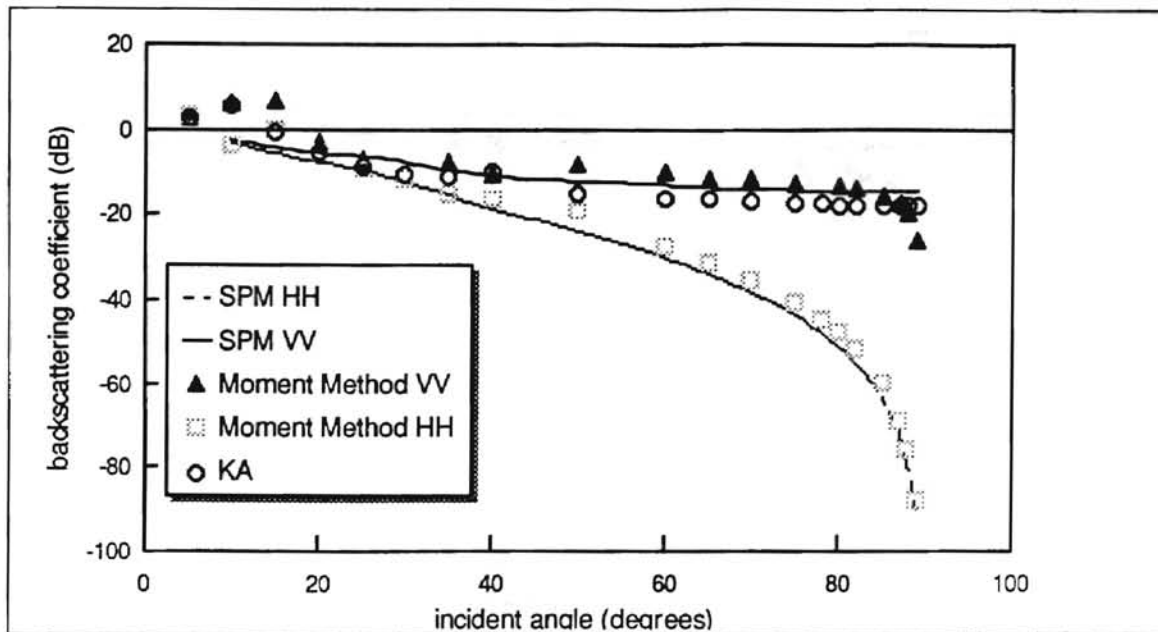| Frequency	RMS Surface Height (in wavelengths)
8GHz	0.0857744
18GHZ	0.1929924
28GHz	0.3002104
38GHz	0.4074284
48GHz	0.5146464
58GHz	0.6218644

Figure 4.1 Backscattering coefficients predicted at 8GHz by the small perturbation method (SPM), periodic surface moment method (PSMM) and Kirchoff approximation (KA) at vertical (VV) and horizontal (HH) polarization. Note that KA yields identical coefficients at HH and VV polarizations. polarizations.
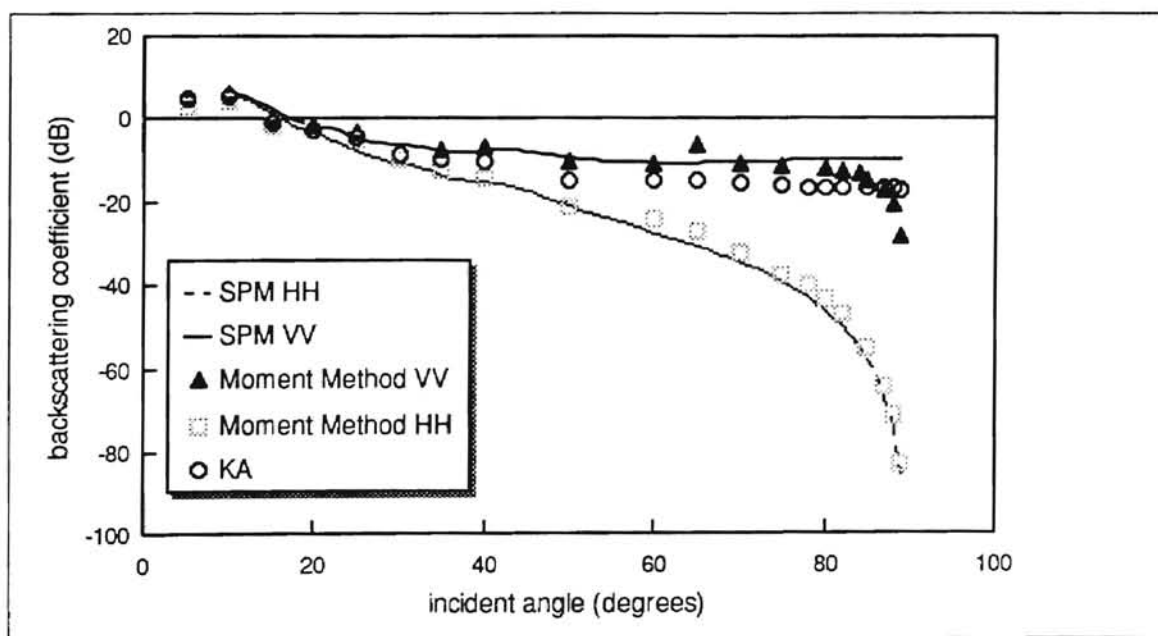
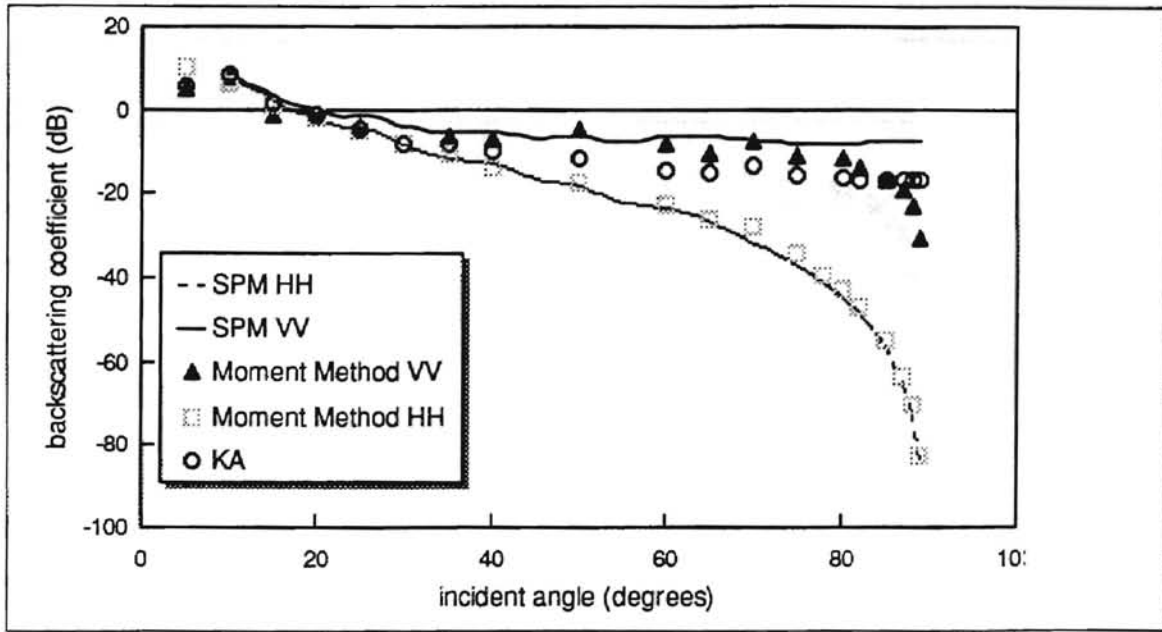

Figure 4.2 Same as 4.1 but at 18GHz

40

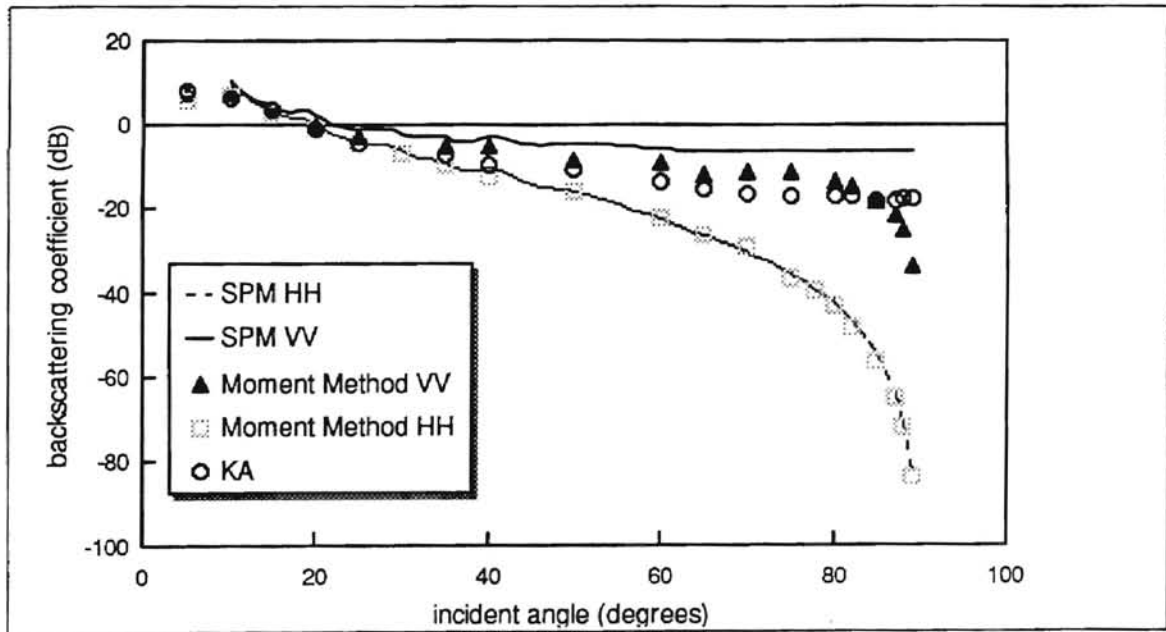**Figure 4.3 same as 4.1 but at 28GHz**
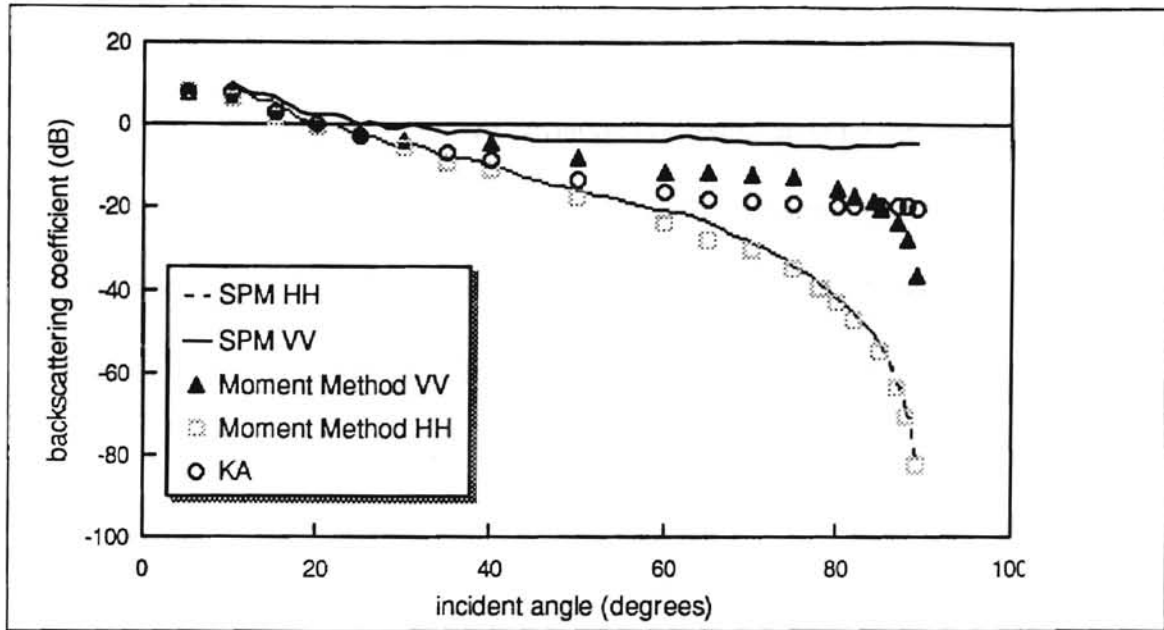

Figure 4.4 same as 4.1 but at 38GHz

41

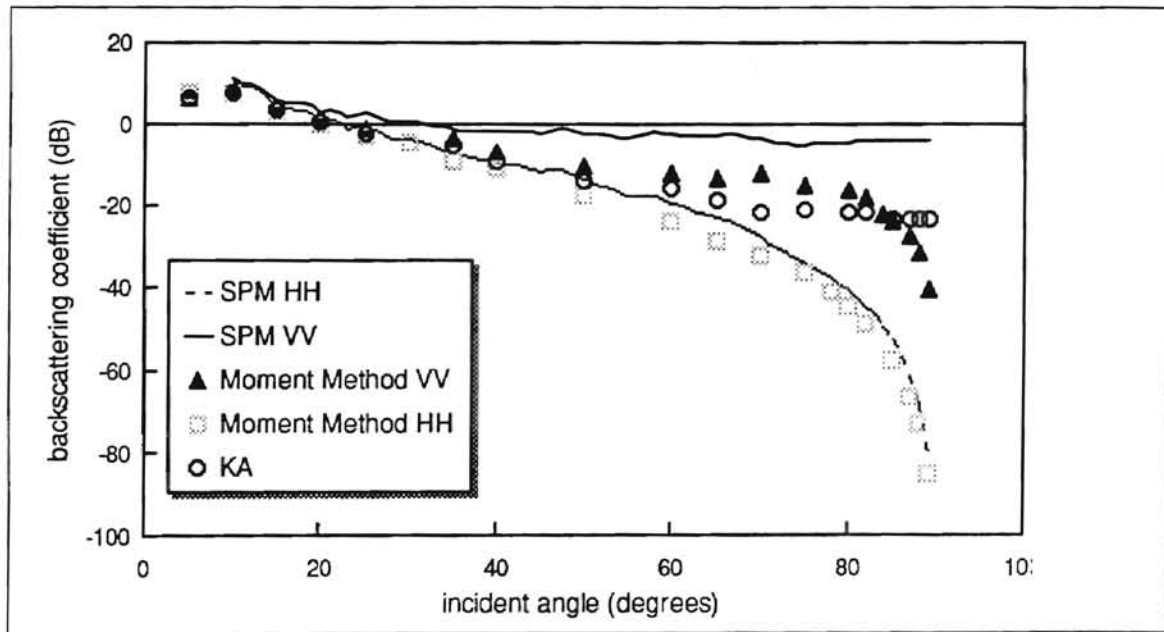**Figure 4.5 same as 4.1 but at 48GHz**

Figure 4.6 same as 4.1 but at 58GHz

Discussion

At 8GHz, the surface standard deviation is 0.086λ, meeting the smallness criteria for SPM to be valid at moderate incidence angles given in chapter two[Ulaby et.al. 1982]. This is confirmed in Figure 4.1 where SPM and PSMM agree to within 3dB at all angles examined above 20° for horizontal polarization and from 20° to 87° incidence at vertical polarization. Above 87° the MM-VV scattering drops rapidly, and is 12dB below the SPM predictions at 89°. The Kirchoff approximation is accurate to within 2dB at all incidence angles below 20°. These results are similar to those found by Chen and West (1995) in their investigation of scattering from small-scale rough surfaces that had Gaussian-weighted roughness spectra..

The operating frequency was increased to 18GHz in Figure 4.2, giving a surface standard deviation of 0.193λ. The rolloff of the SPM-VV scattering now occurs at a smaller incidence angle of 82° most likely due to the increased self shadowing resulting from the greater electromagnetic roughness. The horizontal results still proved accurate to 89° incidence. KA is accurate to 25° at both polarizations at this frequency, slightly higher than at 8GHz, and again, due to the increased surface roughness.

The general trend of the PSMM-VV scattering rolloff beginning at lower incidence and KA scattering being accurate to higher incidence with increasing frequency is continued in Figures 4.3 through 4.6. At 58GHz in Figure 4.6, the surface standard deviation is 0.629λ. Here the strong rolloff in the PSMM-VV occurs at about 75° incidence, reaching a maximum error of more than 25dB at 89°. SPM-HH gives excellent

43

agreement with the corresponding MM results through 88° and overpredicts the scattering

by only 7dB at 89° incidence. This result is not in agreement with the large-scale

roughness results found by Chen and West (1995). This disagreement arises from the fact

that Chen and West used a Gaussian power spectral density to describe the surface

roughness, which includes no Bragg-resonant energy at high frequencies/large roughness.

KA is still valid at this frequency up to about 40°. Note that PSMM yields similar

scattering coefficients at the two polarizations at the smallest incidence angles at all

frequencies, and the maximum angle at which they agree increases with increasing

frequency. This allows KA, which includes no polarization dependence, to accurately

predict the scattering for both polarizations up to these angles.

As discussed earlier, the power spectral density for the experimentally measured

surfaces is in agreement with the power-law spectra sometimes used to describe the ocean

surface. Thus these results are quite different from the scattering from the

Gaussian-weighted spectrum surfaces presented by West and Chen(1995), but similar to

that obtained by West et. al. (1995) when a power law surface was used.

CHAPTER FIVE

CONCLUSIONS

The validity of the small perturbation and Kirchoff approximation models in predicting electromagnetic scattering from rough water surfaces has been examined. The scattering predicted by the models was directly compared with the numerically calculated "exact" scattering from sample water surfaces. Use of a periodic-surface moment method for scattering calculations allowed the comparison at incidence angles up to 89°, considerably higher than that possible using the standard windowed-illumination moment method.

Often the greatest limitation of numerical studies such as this, is the method used to represent the scattering surface. The statistics of the roughness of open water surfaces are not well known and accurate direct measurements of the roughness with resolution fine enough to resolve the small Bragg-resonant ripple waves do not exist. Thus surfaces have typically been generated from idealized roughness spectra that are at best only rough approximations of the actual surface spectra.

In this work, the scattering surfaces were derived from direct measurements of the upwind/downwind slopes of wind-generated water surfaces in a circular wave tank. The slopes were processed to yield several independent, one dimensionally rough scattering surface to which the numerical scattering algorithm was directly applied. While the

45

surfaces are of course also not truly representative of the open sea surface, this approach does allow the Bragg-resonant ripples to be resolved allowing an accurate representation of a very important scattering mechanism with wind-generated water surfaces.

When the frequency was chosen so that the scattering surface roughness was electromagnetically small(8GHz) the small perturbation theory was found to be accurate at incidence angles up to at least 89° for horizontal polarization. At vertical polarization, SPM was accurate to 87° and rolled off sharply at higher incidence. The incidence angle at which this rolloff occurred reduced with increasing frequency down to about 75° at 58GHz, indicating that SPM is valid over a wider range of surface roughness and incidence angles at horizontal polarization. The Kirchoff approximation was found to be accurate at small and moderate grazing angles, with the highest angle of validity increasing with frequency. A surprising result is that KA seems to accurately predict the scattering for vertical polarization up to 85° at 58GHz, with no shadowing correction. These results indicate that the approximate scattering models may be valid over a wider range than previously thought.

REFERENCES

Axline R.M. and Fung A.K., "Numerical Computation of Scattering from perfectly Conducting Random Surface," IEEE Transactions on Antennas and Propagation Vol. AP-26 pp. 482-488. 1978.

Balanis, C.A., *Advanced Engineering Electromagnetics*, New York, John Wiley and Sons 1989.

Balanis, C.A., *Antenna Theory Analysis and Design*, New York, John Wiley and Sons 1982.

Beckman, P., and Spizzichino, A. *The Scattering of Electromagnetic Waves From Rough Surfaces.* Macmillan, New York, 1963.

Breipohl A.M., and Shanmugan K.S., *Random Signals Detection, Estimation and Data Analysis*, New York, John Wiley and Sons 1988.

Broschat, S.L., "The phase perturbation approximation for rough surface scattering from a Pierson-Moskowitz sea surface," IEEE Transactions on Geoscience and Remote Sensing., vol. 31, no 1 pp. 278-283, January 1993.

Brown, Gary S./ "Backscattering from a Gaussian-distributed perfectly conducting rough surface," IEEE Transactions on Antennas and Propogation., vol. AP-26, no. 3, pp. 472 - 481, May 1978.

Chen K.S. and Fung A.K. "A Comparison of Backscattering Models for Rough Surfaces," IEEE Transactions on Geoscience and Remote Sensing. Vol. 33 no. 1 pp. 195-200

Chen M.F., and Fung A.K., "A Numerical Study of the Regions of Validity of the Kirchoff and Small Perturbation Rough Surface Scattering Models," Radio Science, Vol. 23 No. 2 pp. 163 - 170. 1988.

Chen, Ruimin., "Numerical Investigation Of Electromagnetic Scattering From The Ocean Surface At Extreme Grazing Angles," Diss., Oklahoma State University 1993.

Durden, S.L., and J. Vesecky., "A Numerical Study of the Separation Wavenumber in the Two-Scale Scattering Approximation," IEEE Transactions on Geoscience and Remote Sensing., vol. 28, no. 2, pp. 271-272, March 1990.

Fung, A.K., Moore, R.K., and Ulaby, F.T., *Microwave Remote Sensing Volume II*, reading, MA: Addison Wesley, 1982.

Guinard, N.W., "An Experimental Study of a Sea Clutter Model", Proceedings of the IEEE, 58(4), 543-550, 1970.

Harrington R., *Field Computation by Moment of Methods*, Macmillan, New York, 1968.

Jackson D.R. and Thorsos E.L., "The Validity of the Perturbation Approximation for Rough Surface Scattering Using a Gaussian Roughness Spectrum," Journal of the Acoustical Society of America. Vol. 86 No. 3. pp. 261-277. 1988.

Jahne, Bernd, and Klinke, Jochen, "Wave Number Spectra of Short Wind Waves -- Laboratory Results and Extrapolation to the Ocean", Draft copy, June 22, 1994.

Jahne, B. and Shultz H. "Calibration and Accuracy of Optical Slope and Height

Measurements for Short Wind Waves", SPIE Proceedings 1749, in press 1992.

Kim Y., Rodriguez E. and Durden S.L., "A Numerical Assessment of Rough Surface
Scattering Theories: Vertical Polarization," Radio Science Vol. 27 pp. 515-527. 1992.

Kim Y., Rodriguez E. and Durden S.L., "A Numerical Assessment of Rough Surface
Scattering Theories: Horizontal Polarization," Radio Science Vol. 27 pp. 495-513.
1992.

Rice S.O., "Reflection of Electromagnetic Waves from Slightly Rough Surfaces,"
Communications on pure and applied mathematics Vol. 4 pp. 351-378. 1951.

Sturm, J.M., "Iterative Methods For Solving Large Linear Systems In The Moment
Method Analysis Of Electromagnetic Scattering," Thesis, Oklahoma State University
1993.

Thacher, H.T. "Algorithm 215: SHANKS," Communications of the ACM, vol. 6, no. 11,
pp. 662, Nov. 1963

West, James C., and Ruimin Chen, "Analysis of scattering from rough surfaces at small
grazing angles using a periodic-surface moment method," IEEE Transactions on
Geoscience and Remote Sensing., vol. 31, no 1 pp. 278-283, September 1995.

West, James C., "Numerical Prediction of Shadowing in EM Scattering From a Rough
Ocean Wave at Grazing Incidence," currently under review

West, James C. et.al., "The Slightly-Rough Facet Model in Radar Imaging of the ocean
surface," International Journal of Remote sensing, vol. 11, no. 4, pp. 617-637, April
1990.

West, James C., Ruimin Chen, and Brent O'Leary., "Numerical Calculation of Scattering

From Rough Surfaces with Power-Law Spectra Using a Periodic Surface Moment

Method", 1995 Progress in Electromagnetics Research Symposium (PIERS 1995),

Seattle Washington, July 24-28, 1995.

$\overline{L}$

VITA

Brent Sean O'Leary

Candidate for the Degree of

Master of Science

Thesis: A COMPARISON OF SCATTERING RESULTS OBTAINED WITH
THE PERIODIC SURFACE MOMENT METHOD AND SEVERAL
APPROXIMATE SCATTERING THEORIES USING WAVE-TANK
DATA

Major Field: Electrical Engineering

Biographical:

Personal Data: Born in Wichita Kansas, May 26, 1970, the son of Mr. and Mrs.
James Edward O'Leary. Wife Tina, and one son, Chandler.

Education: Graduated from Hooker High School, Hooker Oklahoma, in May 1988;
Received Bachelor of Science Degree in Electrical Engineering from
Oklahoma State University in December, 1993; Completed the requirements
for the Master of Science Degree at Oklahoma State University in July, 1996.

Professional Experience: Electronic Systems Engineer, Lockheed Martin
Vought-Systems, June 1995 to present. Research Assistant, Department of
Electrical Engineering, Oklahoma State University, January 1993 to June 1995;

Professional Memberships: IEEE, NSPE, Eta Kappa Nu and Phi Kappa Phi